Preparation and thermal performance of a novel 1,10-Decanediol - paraffin/expanded graphite composite phase change material for solar thermal utilization

Kai Fu[a], Songping Mo[a,b,*], Qing Li[a], Zicong Zhou[a], Lisi Jia[a,b], Yanping Du[c], Ying Chen[a,b]

[a] *School of Materials and Energy, Guangdong University of Technology, Guangzhou 510006, China.*

[b] *Guangdong Provincial Key Laboratory on Functional Soft Condensed Matter, Guangdong University of Technology, Guangzhou 510006, China.*

[c] *School of Engineering, Lancaster University, Lancaster LA1 4YW, UK*

Abstract The intermittent nature of solar irradiation poses significant challenges to the energy transfer stability of conventional solar-thermal conversion materials. To address this, solar-thermal phase change materials (PCMs) integrate thermal conversion and storage, mitigating temporal and spatial discontinuities of solar energy. However, existing PCMs suffer from limitations such as inadequate solar absorption, leakage, and low phase change enthalpy. In this study, a novel binary eutectic PCM comprising 1,10-decanediol (DDL) and paraffin wax (PW) was synthesized via melt blending. Expanded graphite (EG) was incorporated as a thermal conductivity enhancer and structural support, with a shape-stabilized composite PCM fabricated through vacuum impregnation. The DDL-PW/EG composite achieved a high encapsulation efficiency of 90%, exhibiting a phase change temperature of 63.2 ℃ and a latent heat capacity of 203.9 $kJ \cdot kg^{-1}$. Notably, its thermal conductivity reached 6.89 $W \cdot m^{-1} \cdot K^{-1}$, 13.78 times higher than that of pristine DDL-PW, while maintaining 85% photothermal conversion efficiency. Accelerated thermal cycling tests (200 cycles) revealed negligible degradation in phase change temperature and enthalpy, underscoring exceptional thermal reliability of the composite. Combining robust thermal storage performance with efficient solar-thermal conversion, the DDL-PW/EG composite demonstrates significant potential for advancing solar energy harvesting and storage applications.

[*] Corresponding author.

E-mail address: mosp@ustc.edu.

Keywords: Phase change material, Eutectic, Photothermal, Decanediol, Composite, Thermal conductivity

1. Introduction

The escalating emission of greenhouse gases has intensified global warming, propelling the change to low-carbon energy systems as a pivotal strategy for achieving emission reduction targets [1]. Solar energy, renowned for its abundance, environmental compatibility, and ubiquitous availability, stands out as a leading renewable energy candidate [2]. However, its intermittent nature, both temporally and spatially, poses significant challenges to widespread adoption. To address this, efficient energy storage technologies have emerged as a critical research priority [3, 4]. Among these, thermal energy storage (TES) systems offer a cost-effective and efficient solution, enabling the capture and storage of solar heat during peak irradiance periods for later use during low-irradiance periods, thereby ensuring a stable energy supply [5, 6].

PCMs are particularly advantageous in TES applications due to their ability to store and release substantial latent heat during phase changes, enhancing energy storage density and system efficiency [7, 8]. These properties have driven the extensive application of PCMs in diverse fields, including building climate control [9, 10], solar water heating systems [11, 12], and thermal management of electronic devices [13, 14].

Organic phase change materials, including paraffin, fatty acids, and polyols, have garnered significant research interest due to their high latent heat capacity and minimal corrosivity. Among these, eutectic organic phase change materials, synthesized by combining multiple organic PCMs, offer tailored thermal properties, enabling precise adjustments to melting points and latent heat to address specific application requirements [15]. This adaptability is particularly critical for solar thermal energy storage systems. For instance, Fan et al. [16] developed a myristic acid-paraffin eutectic PCM via melt blending, demonstrating exceptional reliability for latent solar heat storage. Duraipandi et al. [17] further validated the practicality of eutectic PCMs by integrating palmitic acid-decanoic acid blends with solar dryers, extending operational

heating durations and improving system efficiency. Narayanan et al. [18] advanced this field by formulating a paraffin-oleic acid eutectic PCM with nano-graphite additives, showcasing its efficacy in photovoltaic thermal management.

PCMs face critical limitations, including low thermal conductivity, phase-change-induced leakage, and inadequate solar-thermal conversion efficiency, which hinder their broader application in solar energy systems. To address these challenges, there is an urgent demand for composite PCMs with enhanced thermal conductivity, superior solar-thermal conversion performance, and shape stability [19]. Expanded graphite (EG), a three-dimensional thermally conductive additive, has emerged as a promising solution. By leveraging capillary forces and surface tension, EG effectively adsorbs liquid PCMs into its porous structure, forming shape-stabilized composites while simultaneously mitigating leakage and increasing thermal conductivity [20, 21]. For instance, Yan et al. [22] developed an erythritol/EG composite PCM (CPCM) and demonstrated that incorporating 6 wt% EG improved thermal conductivity from 0.60 ± 0.03 $W \cdot m^{-1} \cdot K^{-1}$ (pure erythritol) to 5.97 ± 0.30 $W \cdot m^{-1} \cdot K^{-1}$. Similarly, Tan et al. [23] synthesized a ternary eutectic PCM (hexanediol-dodecanol-caprylic acid) combined with EG via vacuum impregnation. The resulting CPCM achieved a thermal conductivity of 1.8980 $W \cdot m^{-1} \cdot K^{-1}$, 10.25 times higher than the pristine ternary PCM, while reducing phase change time by 10%. Xu et al. [24] engineered a hexadecyl alcohol-palmitic acid/expanded graphite (HA-PA/EG) composite eutectic PCM, which combines a suitable phase change temperature with enhanced thermal conductivity for photovoltaic module temperature regulation. These advancements underscore EG's dual role in enhancing thermal performance and structural reliability.

Despite advancements in PCM research, challenges such as low latent heat at target temperatures remain unresolved. Saturated diols, which exhibit minimal phase separation, high latent heat, negligible volume change, and robust thermal stability, have emerged as promising candidates for TES systems [25]. However, limited studies have explored eutectic mixtures of saturated diols with paraffin wax (PW). This design effectively suppresses the double-peak behavior of paraffin during the phase transition and maximizes the utilization of its latent heat. In this study, we introduce a novel

organic eutectic PCM composed of 1,10-decanediol (DDL) and PW, combined with EG to form a shape-stabilized CPCM via vacuum impregnation. Here, DDL and PW act as the eutectic PCM, while EG enhances thermal conductivity and prevents leakage. The thermal properties, microstructure, and thermal conductivity of the DDL-PW/EG CPCM were systematically characterized using differential scanning calorimetry (DSC), scanning electron microscopy (SEM), and thermal conductivity analyzer. Additionally, simulated solar irradiation experiments were conducted to evaluate its solar absorption capacity and photothermal conversion efficiency. The results reveal that the DDL-PW/EG CPCM achieves a phase change temperature of 63.2 ℃, a high latent heat of 203.9 $kJ \cdot kg^{-1}$, and a thermal conductivity of 6.89 $W \cdot m^{-1} \cdot K^{-1}$, 13.78 times higher than the pristine DDL-PW eutectic. The material also demonstrates low supercooling, exceptional shape stability, and thermal reliability over 200 heating-cooling cycles, alongside a solar-thermal conversion efficiency of 85.0%. These properties collectively position the DDL-PW/EG CPCM as a highly efficient and durable solution for solar TES applications.

2. Experimental

2.1. Materials

PW (C_nH_{2n+2}, RT70HC, 98%) was supplied by Guangzhou Zhongjia New Materials Technology Co., Ltd. 1,10-Decanediol ($C_{10}H_{22}O_2$, 98%) was purchased from Shanghai Macklin Biochemical Technology Co., Ltd. EG (expandable 200-300 times) was obtained from Nanjing Greifa Carbon Materials Co., Ltd. All chemical reagents were of analytical grade and could be used without further purification.

2.2. Preparation of DDL-PW eutectic mixture

A series of DDL-PW binary eutectic mixtures were synthesized using a straightforward physical blending method. To determine the optimal composition, various mass ratios of DDL to PW were screened, ranging from 1:9 to 9:1 (specifically, 1:9, 2:8, 3:7, 4:6, 5:5, 6:4, 7:3, 8:2, and 9:1). Accurately weighed quantities of DDL and PW were transferred into clean, dry glass vials using an analytical balance

(AUY220,Shimadzu). The vials were then placed in a thermostatic magnetic stirrer water bath (DF-101S,YUHUA) maintained at 85 ℃ until the components fully melted, forming a clear and transparent liquid. The mixture was stirred at 500 rpm for 30 min to ensure complete homogeneity. Finally, the resulting binary mixture was cooled to room temperature, after which it was sealed and stored for further use.

2.3. Preparation of DDL-PW/EG CPCMs

To prepare the CPCMs, EG was mixed with the DDL-PW eutectic mixture at varying mass ratios. In each experimental group, the total mass of the PCM was fixed at 10 g. EG was weighed in amounts of 0.6 g, 0.8 g, 1.0 g, and 1.2 g, corresponding to 6 wt%, 8 wt%, 10 wt%, and 12 wt% of the total PCM mass, respectively, and placed into separate beakers. The DDL-PW eutectic mixture was melted at 85 ℃ to form a clear liquid, which was then added to the EG for blending. Due to the excellent compatibility between the DDL-PW eutectic and EG, the mixtures were manually stirred vigorously for 30 min to promote the adsorption of the eutectic mixture into the porous structure of EG. Subsequently, the blended mixtures were placed in a vacuum drying oven at 100 ℃ for 5 h to ensure thorough infiltration of the DDL-PW eutectic into the porous network of EG. This step completed the preparation of the CPCMs.

2.4. Characterization

The morphology of EG and DDL-PW/EG CPCMs was analyzed using a Hitachi SU8010 SEM. Phase change temperatures and latent heat were measured via DSC (DSC3 STAR, Mettler Toledo) under nitrogen at 10 ℃·min^{-1} (30–100 ℃). Thermal history was eliminated by preheating samples to 100 ℃ (20 ℃·min^{-1}) and holding for 2 min. Chemical structures were characterized using Fourier transform infrared spectroscopy (FTIR, Nicolet 6700, Thermo Fisher Scientific; 4000–400 cm^{-1}). Crystallinity was evaluated with an in-situ X-ray diffractometer (XRD, Rigaku Ultima IV X). Thermal conductivity was measured using a Hot Disk TPS 500 S thermal constant analyzer with 7577/5465 probes. Thermal stability was assessed via thermogravimetric analyzer (TGA, SDT Q600) at 10 ℃·min^{-1} (25–600 ℃, nitrogen atmosphere). Thermal cycling reliability was tested over 200 melt-solidify cycles (50–80 ℃) in a BTH-80B chamber, followed by post-cycling DSC analysis. Photothermal

conversion performance was evaluated using a CEL-S500-T5 solar simulator (2000 $W \cdot m^{-2}$) with temperature monitoring via a K-type thermocouple and KEYSIGHT DAQ970A data acquisition system. Table 1 summarizes the accuracy of the devices.

Table 1 Accuracy of the devices.

Device	Measured parameter	Accuracy
DSC	Enthalpy	±3%
Thermal constant analyzer	Thermal conductivity	±5%
BTH-80B chamber	Thermal reliability	±0.5 °C
Thermogravimetric analyzer	Mass	0.001%
Thermocouple	Temperature	±1 °C

3. Results and discussion

3.1. Determination of optimal mass ratio for the DDL-PW eutectic mixture

As shown in Fig. 1, the optimal mass ratio for the DDL-PW binary eutectic material was determined by preparing mixtures with varying DDL/PW compositions and analyzing their thermal properties via DSC. Most DDL-PW mixtures displayed dual endothermic/exothermic peaks, indicating incomplete phase change synchronization. However, at a DDL mass fraction of 60 wt%, a single set of endothermic and exothermic peaks emerged, signaling a eutectic composition with synchronized melting/crystallization behavior. This optimized eutectic PCM demonstrated a melting temperature of 63.8 ℃, a solidification temperature of 59.9 ℃, and corresponding latent heats of 229.1 $kJ \cdot kg^{-1}$ and 228.1 $kJ \cdot kg^{-1}$, respectively. When compared to other eutectic PCMs reported in the literature within the same phase change temperature range, the DDL-PW eutectic PCM exhibits a relatively superior latent heat (see Table 2). This DDL-PW eutectic PCM achieves a good balance between latent heat and phase change temperature, offering significant potential for practical applications.

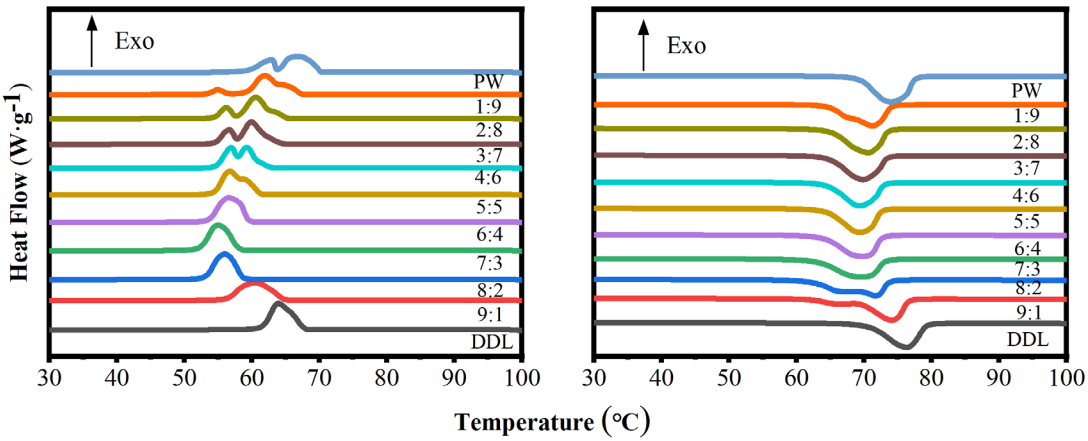

Fig. 1. DSC curves of DDL and PW mixtures with different mass ratios.

Table 2 Thermal properties of DDL-PW eutectic PCM compared with literature data.

Eutectic PCMs	Composition (%)	T_m (°C)	H_m (kJ·kg^{-1})	Refs.
Stearic acid/benzamide	75:25	65.09	200.15	[26]
Stearic acid:n-octanamide	82.7:17.3	63.1	199	[27]
Stearic acid:n-butyramide	70.9:29.1	64.3	198.4	[27]
Stearic acid:suberic acid	96:4	66.4	191.4	[28]
Stearic acid/acetamide	60:40	64.6	194	[29]
DDL-PW	60:40	63.8	229.1	Present

3.2. Microscopic morphology and leakage test of DDL-PW/EG CPCMs

Fig. 2a presents the SEM image of EG, revealing a worm-like microstructure. The graphite nanosheets of EG form irregular pores, which facilitate the adsorption of DDL-PW. Fig. 2b illustrates the micromorphology of EG after vacuum adsorption of DDL-PW, suggesting that DDL-PW fills the internal pores of EG.

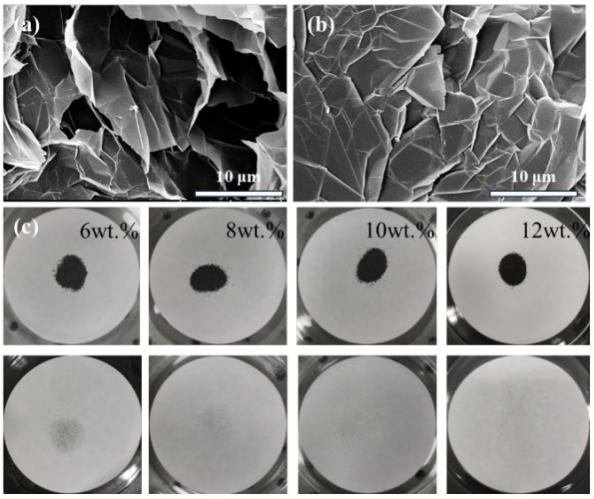

Fig. 2. SEM micrographs of (a) EG and (b) 10 wt% DDL-PW/EG CPCM, (c) photographs of the DDL-PW/EG CPCMs after leakage test.

Leak-proof ability is a crucial performance metric for the practical application of CPCMs [30]. A low mass fraction of EG can lead to leakage issues, compromising the material's effectiveness. However, since EG does not participate in the phase change process itself, increasing its mass fraction reduces the latent heat of the CPCM. To achieve an optimal balance between leakage prevention and maintaining high latent heat, a systematic study was conducted. Specifically, CPCM samples with varying EG mass fractions, including 6 wt%, 8 wt%, 10 wt%, and 12 wt%, were prepared to determine the ideal EG content.

The optimal EG content was evaluated using two complementary approaches. First, we assessed leakage by observing marks left on filter paper after heating. The samples were placed in an 80 ℃ oven for 30 min, and any melted PCM leaking onto the underlying filter paper was visually inspected. Fig. 2c presents photographs taken before and after heating. Notably, the DDL-PW/EG CPCM with 6 wt% EG exhibited significant leakage, leaving clear marks on the filter paper. As the EG content increased, the leakage progressively decreased. When the EG mass fraction reached 10 wt%, leakage was almost entirely suppressed.

Second, the mass loss ratio of the composite was analyzed as another key indicator for determining the optimal EG content. The mass loss ratio was calculated using Eq. (1), and Fig. 3 quantitatively illustrates the mass loss ratios for CPCMs with varying EG contents.

$$L_m(\text{wt\%}) = (M_0 - M_n)/M_0 \times 100\% \quad (1)$$

where L_m represents the mass loss ratio, while M_0 and M_n denote the mass of the sample before and after heating, respectively. The mass loss ratios for EG mass fractions of 6 wt%, 8 wt%, 10 wt%, and 12 wt% were found to be 4.5%, 1.0%, 0.50%, and 0.48%, respectively. When the EG content reached 10 wt% or higher, the mass loss became negligible. In summary, our findings demonstrate that an EG mass fraction of 10 wt% represents the optimal balance between minimizing leakage and maintaining desirable latent heat for the DDL-PW/EG CPCM.

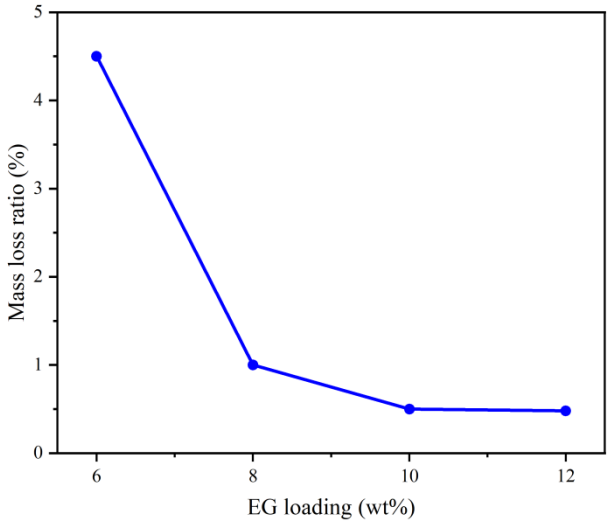

Fig. 3 Mass loss ratios of CPCMs with varying EG contents.

3.3. Chemical composition and crystal structure of DDL-PW/EG CPCMs

To investigate the chemical structure of DDL-PW/EG CPCMs, FTIR was used to characterize PW, DDL, DDL-PW, EG, and the DDL-PW/EG composite. As shown in Fig. 4a, the FTIR spectrum of PW displays absorption peaks at 2913 cm^{-1} and 2845 cm^{-1}, corresponding to asymmetric and symmetric stretching vibrations of $–CH_2$ groups. Peaks at 1464 cm^{-1}, 1057 cm^{-1}, and 722 cm^{-1} are attributed to $–CH_2$ bending, C–C stretching, and $–CH_2$ rocking vibrations, respectively [20]. EG exhibits three characteristic peaks: 3435 cm^{-1} (O–H stretching), 1626 cm^{-1} (C=O stretching), and 1103 cm^{-1} (C–O stretching), reflecting its oxygen-containing polar groups, which enhance compatibility with other polar molecules. For DDL, the FTIR spectrum shows a broad peak at 3412 cm^{-1} (–OH stretching), along with peaks at 2923 cm^{-1} and 2849 cm^{-1} ($–CH_2$/$–CH_3$ stretching), 1050 cm^{-1} (C–O stretching), and 1460–1480 cm^{-1} ($–CH_2$

scissoring) [31]. In the DDL-PW/EG CPCM spectrum, all characteristic peaks of PW and DDL are retained, and no new peaks emerge, confirming that the composite forms via physical adsorption without chemical interactions.

To evaluate chemical compatibility and stability, XRD analysis was performed on PW, DDL, DDL-PW, EG and DDL-PW/EG CPCM (Fig. 4b). PW shows diffraction peaks at 21.8° and 24.7°, while DDL exhibits a high peak at 23.3°. The XRD pattern of DDL-PW retains peaks from both PW and DDL, indicating a physical blend. EG displays a sharp peak at 26.26°. Notably, the XRD pattern of DDL-PW/EG CPCM does not exhibit new peaks, confirming that EG integration is physical and does not disrupt the crystal structure of DDL-PW. These findings demonstrate excellent chemical compatibility among all components.

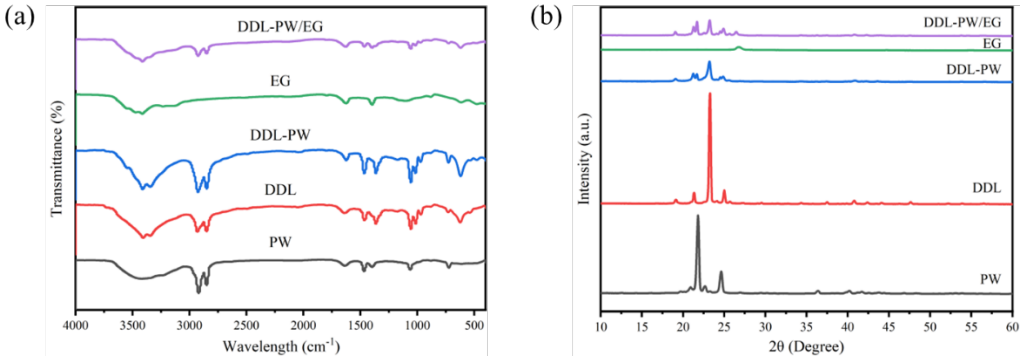

Fig. 4. FT-IR patterns (a) and XRD spectra (b) of PW, DDL, DDL-PW, EG and DDL-PW/EG CPCM.

3.4. Phase change behavior of DDL-PW/EG CPCMs

The phase change behavior of DDL-PW/EG CPCMs was analyzed via DSC. Fig. 5 illustrates the melting and solidification curves of CPCMs with varying EG contents. Notably, all CPCMs exhibit a single endothermic peak during melting and a single exothermic peak during solidification. This consistency confirms the stable eutectic structure in DDL-PW/EG CPCMs and suggests that EG has a negligible impact on their phase change behavior. Since EG remains inert (no phase change between 30 °C and 100 °C), the phase change latent heat of the CPCMs were calculated using Eq. (1) [32].

$$\Delta H_{CPCM,t} = \omega \Delta H_{PCM} \quad (2)$$

where ΔH_{PCM} is the phase change latent heat of DDL-PW, $\Delta H_{CPCM,t}$ is the theoretical phase change latent heat of DDL-PW/EG CPCM, ω is the mass fraction DDL-PW of in the DDL-PW/EG CPCM. As shown in Table 3, the change in melting/solidification temperature of the CPCMs is minimal, indicating that the effect of EG on the phase change temperature is negligible. Evidently, the experimental phase change latent heat of DDL-PW/EG CPCMs is slightly lower than the theoretical value. This discrepancy may be due to the weak physical interactions between the porous structure of EG and DDL-PW. These observations are consistent with reports in the literature [26]. Overall, despite the addition of EG, the latent heat of DDL-PW/EG CPCMs remains high (>200 kJ·kg^{-1}).

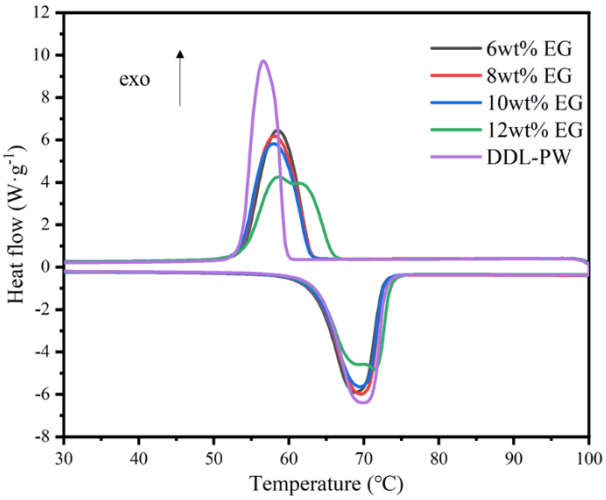

Fig. 5. DSC curves of DDL-PW/EG CPCMs with various EG mass fraction.

Table 3 Phase change properties of DDL-PW CPCMs.

EG fraction	T_m(℃)	H_m(kJ·kg^{-1})	T_f(℃)	H_f(kJ·kg^{-1})	ΔT(℃)
0 wt% (DDL-PW)	63.8	229.1	59.9	228.1	3.9
6 wt%	63.2	212.8	63.1	209.5	0.1
8 wt%	63.2	214.0	63.1	210.9	0.1
10 wt%	63.2	203.9	63.0	201.3	0.2
12 wt%	63.2	203.1	66.0	199.1	-2.8

In PCM applications, supercooling degree (ΔT=T_m-T_f) is an important parameter to evaluate energy storage performance [33]. In practical energy storage scenarios, excessive supercooling can result in delayed and inefficient heat release, thereby

reducing energy utilization efficiency. Notably, the addition of EG significantly reduces the supercooling degree of DDL-PW. This effect can be attributed to the high specific surface area of EG, which provides numerous heterogeneous nucleation sites that facilitate the solidification process. Interestingly, the solidification temperature of the 12 wt% EG sample (as shown in Table 3) was observed to be slightly higher than its melting temperature. This phenomenon can be explained by the definition of the phase change temperatures represented by the onset temperatures. Specifically, the peak temperature of the solidification curve is lower than that of the melting curve (as illustrated in Fig. 5), which is consistent with prior observations. Such behavior has also been reported in previous studies [34, 35]. These studies indicate that the onset temperature is least affected by variations in sample mass or heating rate, making it a reliable representation for the material's melting point. Accordingly, in this work, the phase change temperature refers specifically to the onset temperature, defined as the intersection between the baseline and the tangent to the peak on the heat flow curve [36]. Two additional minor factors may contribute to this observation. First, the addition of EG induces structural changes in the eutectic mixture due to its porous nature, which can influence both melting and solidification temperatures [37]. Second, the discrepancy between melting and solidification temperatures may arise from inherent experimental errors associated with DSC testing [36]. However, such deviations remain well within the acceptable range of experimental uncertainty.

3.5. Thermal conductivity of DDL-PW/EG CPCMs

Thermal conductivity is a critical parameter for PCMs, as it directly governs their energy storage efficiency during charging and discharging cycles. In this study, the thermal conductivity of DDL-PW and DDL-PW/EG CPCMs with varying EG mass fractions was measured (Fig. 6). The pristine DDL-PW PCM exhibited a low thermal conductivity of 0.5 $W \cdot m^{-1} \cdot K^{-1}$, insufficient for practical energy storage applications. However, incorporating EG resulted in an enhancement in thermal conductivity with increasing EG content. For EG mass fractions of 6 wt%, 8 wt%, 10 wt%, and 12 wt%, thermal conductivity values reached 4.31, 6.01, 6.89, and 7.42 $W \cdot m^{-1} \cdot K^{-1}$, respectively,

corresponding to 8.62, 12.02, 13.78, and 14.84 times improvements over pure DDL-PW. This dramatic enhancement is attributed to highly conductive three-dimensional network of EG, which facilitates efficient heat transfer pathways within the composite [38].

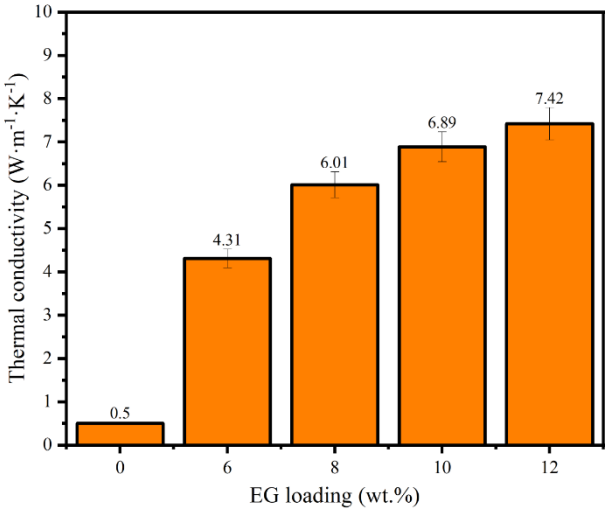

Fig. 6. Thermal conductivity of DDL-PW/EG CPCMs.

As shown in Table 4, the DDL-PW/EG CPCM demonstrates a unique combination of higher latent heat and enhanced thermal conductivity compared to previously reported EG-based CPCMs. This unique performance profile makes it a promising candidate for thermal energy storage systems.

Table 4 Comparison of latent heat of melting and thermal conductivity between present study and reported EG-based CPCMs.

Samples	EG fraction	T_m (°C)	H_m (kJ·kg^{-1})	Thermal conductivity (W·m^{-1}·K^{-1})	Refs
Stearic acid/EG	10	69.27	185.32	3.8	[39]
Acetamide/EG	10	65.91	163.71	2.61	[40]
C18-acid/C18-OH/EG	9	47	143	3.38	[41]
Hexadecanol-Palmitic acid/EG	15	43.2	182.3	5.804	[24]
Stearic acid-benzamide/EG	12	65.48	176.03	4.177	[26]
DDL-PW/EG	10	63.2	203.9	6.89	Present

3.6 TGA analysis of DDL-PW/EG CPCM

The thermal stability of CPCMs is critical for ensuring reliability under high-

temperature conditions. TGA curves for DDL-PW, EG, and DDL-PW/EG CPCM are presented in Fig. 7. Notably, EG exhibits no thermal decomposition below 600 ℃, as indicated by its flat TGA profile. For DDL-PW, initial decomposition begins at 180 ℃, with complete degradation occurring by 330 ℃ . In contrast, the DDL-PW/EG CPCM demonstrates significantly enhanced stability, with initial decomposition delayed to 206 ℃ and final decomposition extended to 350 ℃. These thresholds exceed the operational temperature range of the PCM, confirming that EG incorporation improves thermal durability by raising decomposition temperature.

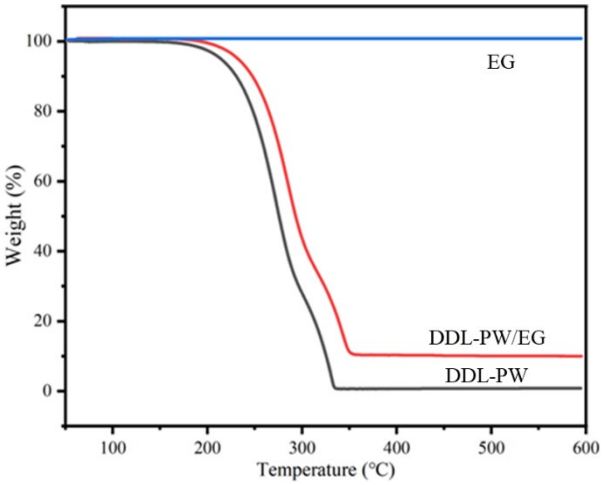

Fig. 7. TGA curves of the DDL-PW, EG and DDL-PW/EG CPCM.

3.7 Thermal reliability of DDL-PW/EG CPCM

For practical applications, thermal reliability is a key indicator of long-term durability for DDL-PW/EG CPCMs. To evaluate this, the thermal properties, chemical composition, and crystal structure of DDL-PW/EG CPCMs were analyzed before and after 200 heating-cooling cycles using DSC, FT-IR, and XRD.

As shown in Fig. 8a, the DSC curves of the CPCM before and after cycling are nearly identical. After 200 cycles, the melting and solidification latent heats remain 198.5 $kJ \cdot kg^{-1}$ and 195.4 $kJ \cdot kg^{-1}$ (Table 5), respectively, representing reductions of just 2.6% and 2.9% compared to initial values. These negligible losses confirm stable phase-change behavior over extended cycling.

FT-IR spectra (Fig. 8b) of the cycled CPCM show no new peaks or significant shifts, indicating preserved chemical integrity. Similarly, XRD patterns (Fig. 8c) reveal

unchanged peak positions before and after cycling, verifying the stability of the crystal structure. Collectively, these results demonstrate that the DDL-PW/EG CPCM maintain excellent thermal and chemical stability under prolonged thermal cycling, making them highly promising for solar thermal energy applications.

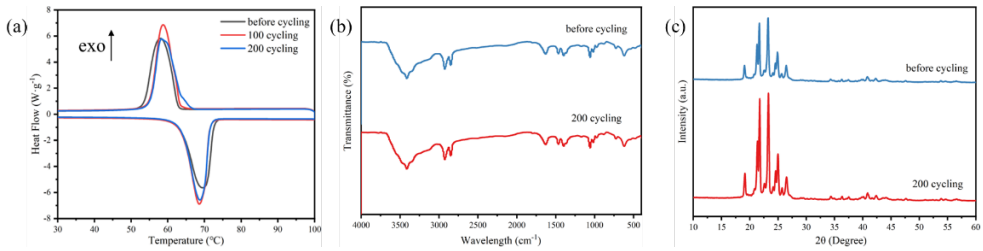

Fig. 8. DSC curves (a), FT-IR spectra (b) and XRD spectra (c) of DDL-PW/EG CPCM before and after 200 cycles.

Table 5 Phase change properties of DDL-PW/EG after 200 heating-cooling cycles.

Cycle	T_m(℃)	H_m(kJ·kg^{-1})	T_f(℃)	H_f(kJ·kg^{-1})
1	63.2	203.9	63.0	201.3
100	63.5	204.2	63.6	200.1
200	63.4	198.5	64.7	195.4

3.8 Photothermal conversion performance of DDL-PW/EG CPCM

To assess the practical viability of the synthesized CPCMs, photothermal conversion performance was evaluated under simulated solar irradiation. Figure 9 illustrates the temperature response profiles of DDL-PW and DDL-PW/EG CPCMs during illumination. For the DDL-PW/EG CPCM, a distinct temperature plateau between 62–68 ℃ was observed, lasting ~460 s. This plateau corresponds to latent heat storage during phase change, where simulated solar energy is absorbed and converted into thermal energy. Post-phase change, the CPCM's temperature continued to rise to ~75 ℃ until the light source was turned off.

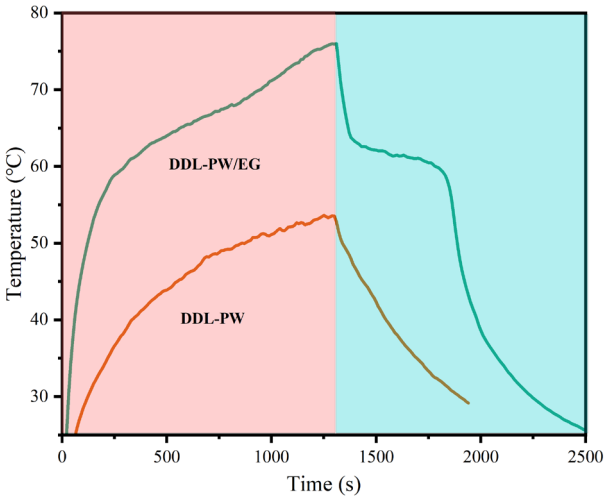

Fig. 9. (a) Schematic diagram of photothermal conversion of DDL-PW/EG CPCM, (b) Photothermal conversion curves of DDL-PW and DDL-PW/EG CPCM.

Upon turning off the light, the CPCM underwent a cooling and heat-release process, exhibiting a solidification plateau at ~65 °C. In contrast, pure PW showed minimal temperature increase, failing to reach its phase change threshold and storing only sensible heat.

The photothermal conversion efficiency (η) was calculated using Eq. (3) [5]:

$$\eta=(m\Delta H_m)/(\rho S(t_2- t_1)) \quad (3)$$

where m is the mass of the sample. The symbols ΔH_m (melting enthalpy of the sample, $kJ\cdot kg^{-1}$), ρ (light source intensity, $W\cdot m^{-2}$), S (sample surface area, m^2), t_1 (phase change onset time, s), and t_2 (phase change end time, s) represent key parameters for evaluating photothermal performance. Calculations reveal that the DDL-PW/EG CPCM achieves a photothermal conversion efficiency of 85.0%. Notably, the incorporation of EG significantly enhances this efficiency. This improvement stems from EG's dual role as an efficient light absorber and thermal conductivity enhancer. The graphite structure effectively captures sunlight, converts solar energy into thermal energy, and facilitates rapid heat transfer within the composite, enabling efficient thermal energy storage and release [42]. As shown in Table 6, the DDL-PW/EG CPCM outperforms other solar thermal utilization materials by combining high thermal storage density with moderate photothermal efficiency. These properties demonstrate its exceptional capability for sunlight absorption and thermal management, positioning it as an ideal candidate for solar energy harvesting, utilization, and storage systems.

Table 6 Comparison of thermal storage density and photothermal conversion efficiency of various types of carbon-based phase change composites.

PCM	Skeleton	H_m(kJ·kg^{-1})	η(%)	Refs.
Lauric acid-stearic acid	Carbon-decorated diatomite matrix	70.07	94.83	[5]
Stearic acid	Surface-decorated graphitic carbon foam	167.60	90.14	[43]
Octadecanol	NiCo@EG	168.3	98.71	[44]
Polyethylene glycol	Ag@reduced graphene oxide-carbonize melamine foam	157.7	90.5	[45]
Paraffin wax	Thermoplastic elastomer/Carbon nanotube	180	96.17	[46]
PW-DDL	EG	203.9	85.0	Present

4. Conclusions

In this study, a novel binary eutectic PCM, DDL-PW, was synthesized. To enhance performance, EG, a highly conductive and porous material, was incorporated to prepare DDL-PW/EG CPCMs with varying EG mass fractions. Leakage tests confirmed a maximum DDL-PW loading capacity of 90 wt% in the composite. The optimized DDL-PW/EG CPCM exhibited a melting temperature of 63.2 ℃, a solidification temperature of 63.0 ℃, and corresponding latent heats of 203.9 kJ·kg^{-1} and 201.3 kJ·kg^{-1}, respectively. With an initial thermal decomposition threshold of 206 ℃, the CPCM demonstrates robust thermal stability for solar applications.

Notably, the integration of 10 wt% EG increased thermal conductivity to 6.89 W·m^{-1}·K^{-1}, 13.78 times higher than pure DDL-PW, while maintaining excellent chemical and crystalline compatibility between components. The CPCM achieved a photothermal conversion efficiency of 85.0%. Furthermore, after 200 heating-cooling cycles, no significant degradation in phase change temperature, latent heat, chemical structure, or crystallinity was observed, underscoring its exceptional thermal reliability. These combined properties—high energy storage density, rapid heat transfer, and long-term stability—make the DDL-PW/EG CPCM particularly well-suited for applications such as solar water heating and building climate control.

CRediT authorship contribution statement

Kai Fu: Investigation, Methodology, Writing-original draft. **Songping Mo**: Conceptualization, Funding acquisition, Project administration, Supervision, Writing-review & editing. **Qing Li**: Investigation. **Zicong Zhou**: Investigation. **Lisi Jia**: Writing-review & editing. **Yanping Du**: Writing-review & editing. **Ying Chen**: Resources.

Declaration of Competing Interests

The authors declare no competing financial interest.

Data availability

Data will be made available on request.

Acknowledgments

This work was supported by the National Natural Science Foundation of China (grant number 51976040).

Reference

[1] H. Fei, Q. He, W. Du, P. Li, J. Zhou, Y. Pan, X. Liang, Structural characteristics and thermal performances of capric acid-stearic acid-octadecanol adsorbed into porous expanded graphite under vacuum condition, J. Energy Storage 72 (2023) 108326, https://doi.org/10.1016/j.est.2023.108326.

[2] H. Lei, X. Wang, Y. Li, H. Xie, W. Yu, Organic-inorganic hybrid phase change materials with high energy storage density based on porous shaped paraffin/hydrated salt/expanded graphite composites, Energy 304 (2024) 132169, https://doi.org/10.1016/j.energy.2024.132169.

[3] P. Zhang, Y. Wang, Y. Qiu, H. Yan, Z. Wang, Q. Li, Novel composite phase change materials supported by oriented carbon fibers for solar thermal energy conversion and storage, Appl. Energy 358 (2024) 122546, https://doi.org/10.1016/j.apenergy.2023.122546.

[4] Z. Chai, M. Fang, X. Min, Composite phase-change materials for photo-thermal conversion and energy storage： A review, Nano Energy 124 (2024) 109437, https://doi.org/10.1016/j.nanoen.2024.109437.

[5] C. Li, M. Wang, B. Xie, Y.-L. He, Carbon-decorated diatomite stabilized lauric acid-stearic acid as composite phase change materials for photo-to-thermal conversion and storage, Renew. Energy 229 (2024) 120731, https://doi.org/10.1016/j.renene.2024.120731.

[6] K. Jiao, L. Lu, T. Wen, Q. Wang, Endowing photothermal materials with latent heat storage: A state-of-art review on photothermal PCMs, Chem. Eng. J. 500 (2024) 156498,

https://doi.org/10.1016/j.cej.2024.156498.
[7] B. Hu, J. Li, X. Du, Z. Zhang, H. Wang, NH4Al(SO4)2·12H2O-Na2SO4 eutectic-based phase change materials with excellent light absorbance, enhanced thermal conductivity, and high latent heat performance, J. Energy Storage 99 (2024) 113349, https://doi.org/10.1016/j.est.2024.113349.
[8] L. Lv, S. Huang, K. Cen, H. Zhou, Experimental study of screening polyols and their binary eutectic phase change materials for long-term thermal energy storage, J. Clean. Prod. 399 (2023) 136636, https://doi.org/10.1016/j.jclepro.2023.136636.
[9] C. Alkan, E.H. Alakara, S. Alay Aksoy, İ. Demir, Cement mortar composites including 1-tetradecanol@PMMA Pickering emulsion particles for thermal energy management of buildings, Chem. Eng. J. 476 (2023) 146843, https://doi.org/10.1016/j.cej.2023.146843.
[10] J. Cheng, Y. Zhou, D. Ma, S. Li, F. Zhang, Y. Guan, W. Qu, Y. Jin, D. Wang, Preparation and characterization of carbon nanotube microcapsule phase change materials for improving thermal comfort level of buildings, Constr Build Mater. 244 (2020) 118388, https://doi.org/10.1016/j.conbuildmat.2020.118388.
[11] X. Man, H. Lu, Q. Xu, C. Wang, Z. Ling, Preparation and thermal property enhancement of sodium acetate trihydrate-lithium chloride-potassium chloride expanded graphite composite phase change materials, Sol. Energy Mater Sol. Cells 266 (2024) 112695, https://doi.org/10.1016/j.solmat.2024.112695.
[12] M. Abdolahimoghadam, M. Rahimi, New hybrid nano- and bio-based phase change material containing graphene-copper particles hosting beeswax-coconut oil for solar thermal energy storage: Predictive modeling and evaluation using machine learning, Energy 307 (2024) 132604, https://doi.org/10.1016/j.energy.2024.132604.
[13] M. Zhi, R. Fan, L. Zheng, S. Yue, Z. Pan, Q. Sun, Q. Liu, Experimental investigation on hydrated salt phase change material for lithium-ion battery thermal management and thermal runaway mitigation, Energy 307 (2024) 132685, https://doi.org/10.1016/j.energy.2024.132685.
[14] J.-X. Wang, J. Qian, N. Wang, H. Zhang, X. Cao, F. Liu, G. Hao, A scalable micro-encapsulated phase change material and liquid metal integrated composite for sustainable data center cooling, Renew. Energy 213 (2023) 75-85, https://doi.org/10.1016/j.renene.2023.05.106.
[15] S. Chang, L. Zhang, X. Li, B. Liu, Y. Meng, H. Hu, Experimental study of novel paraffin-fatty acid eutectic mixtures for thermal management of electronic devices, J. Energy Storage 84 (2024) 110846, https://doi.org/10.1016/j.est.2024.110846.
[16] Z. Fan, Y. Zhao, X. Liu, Y. Shi, D. Jiang, Thermal properties and reliabilities of myristic acid-paraffin wax binary eutectic mixture as a phase change material for solar energy storage, RSC Adv 12 (2022) 12303-12309, https://doi.org/10.1039/d1ra09238c.
[17] S. Duraipandi, S. A, Investigation on the performance of a natural convection solar dryer with novel palmitic and sebacic acid eutectic phase change material for thermal energy storage applications, J. Energy Storage 77 (2024) 109908, https://doi.org/10.1016/j.est.2023.109908.
[18] S.S. Narayanan, A. Kardam, V. Kumar, N. Bhardwaj, D. Madhwal, P. Shukla, A. Kumar, A. Verma, V.K. Jain, Development of sunlight-driven eutectic phase change

material nanocomposite for applications in solar water heating, Resource-Efficient Technologies 3 (2017) 272-279, https://doi.org/10.1016/j.reffit.2016.12.004.
[19] S.-Y. Li, T. Yan, K.-W. Wang, T. Xie, W.-G. Pan, Paraffin wax@TiO2 phase change microcapsules in SiC-doped for solar energy conversion and thermal storage, Sol. Energy Mater Sol. Cells 282 (2025) 113395, https://doi.org/10.1016/j.solmat.2024.113395.
[20] R. Zheng, H. Zhou, C. Li, J. Li, Synergistic phase change and heat conduction of low melting-point alloy microparticle additives in expanded graphite shape-stabilized organic phase change materials, Chem. Eng. J. 482 (2024) 149009, https://doi.org/10.1016/j.cej.2024.149009.
[21] X. Chen, P. Cheng, Z. Tang, X. Xu, H. Gao, G. Wang, Carbon-Based Composite Phase Change Materials for Thermal Energy Storage, Transfer, and Conversion, Adv Sci 8 (2021) 2001274, https://doi.org/10.1002/advs.202001274.
[22] K. Yan, L. Qiu, Y. Feng, Erythritol/expanded graphite form-stable phase change materials with excellent thermophysical properties, J. Energy Storage 68 (2023) 107667, https://doi.org/10.1016/j.est.2023.107667.
[23] S. Tan, X. Zhang, Preparation of organic ternary phase change materials for fruit and vegetable cold chain logistics, J. Energy Storage 108 (2025) 115067, https://doi.org/10.1016/j.est.2024.115067.
[24] T. Xu, R. He, G. Fan, D. Zhang, J. Zhang, Y. Du, W. Zhou, J. Yang, Hexadecanol-palmitic acid/expanded graphite eutectic composite phase change material and its application in photovoltaic panel, Sol. Energy Mater Sol. Cells 273 (2024) 112934, https://doi.org/10.1016/j.solmat.2024.112934.
[25] L. Han, G. Ma, S. Xie, J. Sun, Y. Jia, Y. Jing, Thermal properties and stabilities of the eutectic mixture: 1,6-hexanediol/lauric acid as a phase change material for thermal energy storage, Appl. Therm. Eng. 116 (2017) 153-159, https://doi.org/10.1016/j.applthermaleng.2017.01.082.
[26] G. Ma, J. Sun, Y. Zhang, Y. Jing, Y. Jia, Preparation and thermal properties of stearic acid-benzamide eutectic mixture/expanded graphite composites as phase change materials for thermal energy storage, Powder Technol. 342 (2019) 131-140, http://10.1016/j.powtec.2018.09.074.
[27] G. Ma, S. Liu, S. Xie, Y. Jing, Q. Zhang, J. Sun, Y. Jia, Binary eutectic mixtures of stearic acid-n-butyramide/n-octanamide as phase change materials for low temperature solar heat storage, Appl. Therm. Eng. 111 (2017) 1052-1059, http://10.1016/j.applthermaleng.2016.10.004.
[28] G. Ma, J. Sun, S. Xie, Z. Wang, Y. Jing, Y. Jia, Solid-liquid phase equilibria of stearic acid and dicarboxylic acids binary mixtures as low temperature thermal energy storage materials, J. Chem. Thermodyn. 120 (2018) 60-71, https://10.1016/j.jct.2018.01.008.
[29] G. Ma, L. Han, J. Sun, Y. Jia, Thermal properties and reliability of eutectic mixture of stearic acid-acetamide as phase change material for latent heat storage, J. Chem. Thermodyn. 106 (2017) 178-186, https://10.1016/j.jct.2016.11.022.
[30] Z.-c. Tang, Y.-l. Liu, Z.-j. Huang, Q. Wang, D.-x. Sun, J.-h. Yang, X.-d. Qi, Y. Wang, Hierarchical carbon foams with tunable MOF nanostructure for improving solar-

thermal conversion performance of phase change materials, Carbon 237 (2025) 120161, https://10.1016/j.carbon.2025.120161.
[31] J. Shen, Z. Cai, C. Wang, X. Liu, R. Zheng, Preparation and thermal performances of 1, 10-decanediol-stearic acid eutectic as phase change material, Thermochim. Acta 690 (2020) 178648, https://doi.org/10.1016/j.tca.2020.178648.
[32] Z. Fan, Y. Zhao, X. Liu, Y. Shi, D. Jiang, Development of a new composite material for building energy storage based on lauric acid-palmitic acid-paraffin ternary eutectic and expanded perlite, J. Energy Storage 53 (2022) 105136, https://doi.org/10.1016/j.est.2022.105136.
[33] A. Safari, R. Saidur, F.A. Sulaiman, Y. Xu, J. Dong, A review on supercooling of Phase Change Materials in thermal energy storage systems, Renew. Sust. Energ. Rev. 70 (2017) 905-919, https://doi.org/10.1016/j.rser.2016.11.272.
[34] N. Zhang, Y. Yuan, Y. Du, X. Cao, Y. Yuan, Preparation and properties of palmitic-stearic acid eutectic mixture/expanded graphite composite as phase change material for energy storage, Energy 78 (2014) 950-956, https://10.1016/j.energy.2014.10.092.
[35] M.H. Zahir, S.A. Mohamed, R. Saidur, F.A. Al-Sulaiman, Supercooling of phase-change materials and the techniques used to mitigate the phenomenon, Appl. Energy 240 (2019) 793-817, https://10.1016/j.apenergy.2019.02.045.
[36] H. Fatahi, J. Claverie, S. Poncet, Thermal Characterization of Phase Change Materials by Differential Scanning Calorimetry: A Review, Appl. Sci. 12 (2022) 12019, https://10.3390/app122312019.
[37] L. Zhao, Q. Yu, M. Li, Y. Zhang, Y. Wang, D. Zhan, S. Jin, Y. Huang, Preparation and thermal properties of low-temperature composite phase-change materials based on a binary eutectic mixture with expanded graphite: Effect of particle size and mass fraction, Journal of Energy Storage 40 (2021) 102778, https://10.1016/j.est.2021.102778.
[38] G. Cheng, Z. Wang, X. Wang, Y. He, All-climate thermal management structure for batteries based on expanded graphite/polymer composite phase change material with a high thermal and electrical conductivity, Appl. Energy 322 (2022) 119509, https://doi.org/10.1016/j.apenergy.2022.119509.
[39] H. Gao, N. Bing, H. Xie, W. Yu, Energy harvesting and storage blocks based on 3D oriented expanded graphite and stearic acid with high thermal conductivity for solar thermal application, Energy 254 (2022) 124198, https://doi.org/10.1016/j.energy.2022.124198.
[40] L. Xia, P. Zhang, Thermal property measurement and heat transfer analysis of acetamide and acetamide/expanded graphite composite phase change material for solar heat storage, Sol. Energy Mater Sol. Cells 95 (2011) 2246-2254, https://doi.org/10.1016/j.solmat.2011.03.031.
[41] Z. An, H.J.M. Pea, X. Du, J. Wu, D. Zhang, Preparation and characteristics optimization of octadecanoic acid/octadecanol/expanded graphite based composite phase change materials for energy storage, J. Energy Storage 55 (2022) 105598, https://doi.org/10.1016/j.est.2022.105598.
[42] Q. Zhang, H. Wang, Z. Ling, X. Fang, Z. Zhang, RT100/expand graphite composite phase change material with excellent structure stability, photo-thermal performance and

good thermal reliability, Sol. Energy Mater Sol. Cells 140 (2015) 158-166, https://doi.org/10.1016/j.solmat.2015.04.008.
[43] Y. Zhou, J. Zeng, Y. Guo, H. Chen, T. Bi, Q. Lin, Three-dimensional hierarchical porous carbon surface-decorated graphitic carbon foam/stearic acid composite as high-performance shape-stabilized phase change material with desirable photothermal conversion efficiency, Appl. Energy 352 (2023) 121995, https://doi.org/10.1016/j.apenergy.2023.121995.
[44] Z. Wu, J. Niu, Z. Liu, L. Li, W. Zhang, W. Yuan, NiCo@EG-based composite PCMs with boosted thermal conductivity and photothermal conversion efficiency for solar energy harvesting, Sol. Energy Mater Sol. Cells 278 (2024) 113151, https://doi.org/10.1016/j.solmat.2024.113151.
[45] W. Chen, L. Jiang, X. Hu, A shape-stabilized and thermally enhanced composite phase change material based on Ag@rGO-CMF three-dimensional porous skeleton, J. Energy Storage 114 (2025) 115751, https://doi.org/10.1016/j.est.2025.115751.
[46] X. Kong, X. Liu, J. Yuan, J. Xu, J. Han, Composite phase change materials with thermal-flexible and efficient photothermal conversion properties for solar thermal management, J. Energy Storage 78 (2024) 110027, https://doi.org/10.1016/j.est.2023.110027.